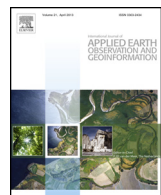




Contents lists available at ScienceDirect

International Journal of Applied Earth Observation and Geoinformation

journal homepage: www.elsevier.com/locate/jag



The effect of atmospheric and topographic correction on pixel-based image composites: Improved forest cover detection in mountain environments



Steven Vanonckelen*, Stef Lhermitte, Anton Van Rompaey

Division of Geography, Katholieke Universiteit Leuven, Celestijnlaan 200E, BE-3001 Heverlee, Belgium

ARTICLE INFO

Article history:

Received 9 June 2014

Accepted 9 October 2014

Keywords:

Forest cover mapping
Classification accuracy assessment
Topographic correction
Landsat
Pixel-based compositing
Mountain areas

ABSTRACT

Quantification of forest cover is essential as a tool to stimulate forest management and conservation. Image compositing techniques that sample the most suited pixel from multi-temporal image acquisitions, provide an important tool for forest cover detection as they provide alternatives for missing data due to cloud cover and data discontinuities. At present, however, it is not clear to which extent forest cover detection based on compositing can be improved if the source imagery is firstly corrected for topographic distortions on a pixel-basis. In this study, the results of a pixel compositing algorithm with and without preprocessing topographic correction are compared for a study area covering 9 Landsat footprints in the Romanian Carpathians based on two different classifiers: Maximum Likelihood (ML) and Support Vector Machine (SVM). Results show that classifier selection has a stronger impact on the classification accuracy than topographic correction. Finally, application of the optimal method (SVM classifier with topographic correction) on the Romanian Carpathian Ecoregion between 1985, 1995 and 2010 shows a steady greening due to more afforestation than deforestation.

© 2014 Elsevier B.V. All rights reserved.

Introduction

The Millennium Development Goals Report (2013) stated that accelerated progress and actions are needed for forest conservation. Forest cover changes affect crucial ecosystem services, such as water supply, biodiversity, carbon storage, and climate regulation (Foley et al., 2005). Assessing the rate and spatial pattern of forest cover change is challenging since large forests are present in rather inaccessible and rough mountain areas (Lambin and Geist, 2006). Multiple efforts have been made to quantify global forest cover changes and forest transitions (Hansen and DeFries, 2004; Meyfroidt and Lambin, 2011; FAO, 2012). These global inventories were either sample-based or based on coarse spatial resolution data (Hansen et al., 2013). Moreover, time-series analysis of forest cover change based on high resolution satellite data have been performed in different countries, e.g. Indonesia (Broich et al., 2011), United States of America (Kennedy et al., 2010; Hansen et al., 2011), Democratic Republic of Congo (Potapov et al., 2012), and Romania (Griffiths et al., 2013b). In contrast, Hansen et al. (2013) presented a global forest cover change inventory based on high resolution

satellite data. Remote sensing techniques are privileged monitoring tools and yet suffer from methodological challenges that need to be resolved by correction methods (Lhermitte et al., 2011a; Balthazar et al., 2012).

The opening of the Landsat archive provides opportunities to reconstruct forest cover changes for large areas on a 30–60 m spatial scale (Loveland and Dwyer, 2012; Giri et al., 2013; Hansen et al., 2013). The use of the Landsat archive with 185 km × 185 km footprint size and a 16-day repeat cycle, however, poses several challenges, ranging from image mosaicking over large areas that cover more than one footprint, to optimal data selection due to cloud cover (Ju and Roy, 2008; Lhermitte et al., 2011b; Griffiths et al., 2013a) and data discontinuities due to sensor or data related errors (e.g. the failure of scan line correction in Landsat 7; Arvidson et al., 2006). Moreover, optimal processing is essential to obtain consistent reflectance values for each Landsat image, where processing methods range from cloud/shadow/water screening and quality assessment, and image normalization for atmospheric conditions and surface anisotropy (Potapov et al., 2011, 2012; Hansen et al., 2013) to physically based atmospheric and topographic correction methods (Minnaert, 1941; Teillet et al., 1982; Berk et al., 1998; Meyer et al., 1993; Jensen, 1996; Richter, 1996; Vermote et al., 1997; Veraverbeke et al., 2010). More recent, comparisons in the performance of different combinations of atmospheric and

* Corresponding author. Tel.: +32 496 366342.

E-mail address: steven.vanonckelen@ine.vlaanderen.be (S. Vanonckelen).

topographic corrections have been made (Riano et al., 2003; Vincini and Frazzi, 2003; Vicente-Serrano et al., 2008; Gao and Zhang, 2009; Vanonckelen et al., 2013, 2014). Finally, the processed Landsat images can be used to detect changes on the original Landsat footprints or on composites derived from the Landsat data, where the latter data have the advantage that they (i) allow solutions over large areas for missing data due to cloud cover and data discontinuities, (ii) avoid artificial partitioning into footprint, (iii) increase observation frequency by across track overlap exploitation (Masek et al., 2006).

Pixel-based image compositing (PBIC), which was initially developed for wide-swath sensor data with clouds (Holben, 1986; Cihlar et al., 1994), selects the most suitable pixel or set of pixel values for each location from a series of available source images. Initial PBIC methods aimed at developing cloud-free composites and implemented the parameter ‘distance from cloud’ as a criterion (Hansen et al., 2008; Roy et al., 2010). Other PBIC methods were developed for the removal of the missing lines in Landsat-7 imagery (Goward et al., 1999; Arvidson et al., 2001, 2006). In 2010, Kennedy et al. presented the Landsat-based detection of trends in disturbance and recovery (LandTrendr) approach which implements change detection algorithms to perform temporal segmentation and fitting of Landsat time series. Griffiths et al. (2013a) presented a large scale forest cover change mapping across the entire Carpathians between 2000 and 2010. The most recent worldwide forest inventory was performed between 2000 and 2012 by Hansen et al. (2013) and used per-pixel set of cloud-free Landsat observations that was normalized for atmospheric conditions and surface anisotropy but not physically corrected for atmospheric or topographic effects. Pixel-based image compositing clearly offers new possibilities for large scale analysis of land and forest cover dynamics. The homogeneous image composites can be classified and analyzed in a single operation resulting in consistent forest cover (change) maps. In general, the impact of a topographic pre-processing method on the results of a PBIC has not been studied. At present, it is unknown to what extent the results of PBIC can be improved if topographic preprocessing is applied on the source images.

Therefore, in this study a pixel-based topographic correction is integrated in the compositing algorithm of Griffiths et al. (2013a) with the objective to (i) assess the impact of topographic correction on classification accuracy of PBICs, and (ii) compare the effect of topographic correction with different classifiers. Within this framework, a large area mapping was performed on the Romanian Carpathian mountains.

Materials and methods

Study area

The study area consists of nine Landsat footprints ($\pm 107,000 \text{ km}^2$) in the Romanian part of the Carpathian Ecoregion, which constitutes more than half of the total Carpathian region (Fig. 1) and contains about 60% of the Carpathian forest cover (Webster et al., 2001). The study area is characterized by mountainous terrain with elevations up to 2544 m and a temperate-continental climate. The growing season is between April and October, and varies in response to annual rainfall and elevation (Rotzer and Chmielewski, 2001). Both temperature and precipitation are highly inversely correlated with elevation. This mountain area is characterized by a mean annual temperature of $\pm 7^\circ\text{C}$ and a mean annual rainfall ranging between 750 and 1400 mm (Mihai et al., 2007; Müller et al., 2009). Warm summers alternate with cold winters and high precipitation rates, mostly as snow. In summer, showers and thunderstorms occur frequently,

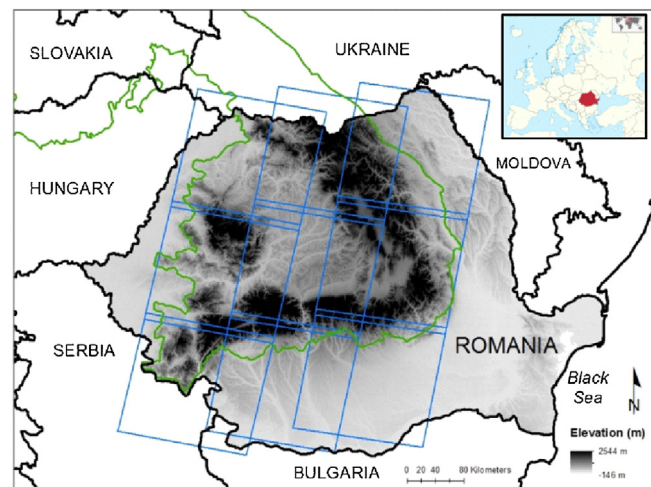


Fig. 1. Location of Romania in eastern Europe and indication of the Carpathian Ecoregion (irregular polygon) and the nine Landsat footprints comprising the Romanian Carpathian Ecoregion (rectangles). Romania was overlaid with the Shuttle Radar Topography Mission elevation data.

reaching peak intensity in June (Mihai et al., 2007). The bedrock in this area consists of crystalline schist, sedimentary rock deposits as limestone and volcanic layers (Griffiths et al., 2013a). Major soils include *Podzols* in the mountain zone and *Cambisols* in the foothill zone (FAO/UNESCO/WRB, 1998).

Data and methodology

Satellite and elevation data

Landsat imagery was selected from the Landsat archive based on two criteria. First, all available Landsat TM and ETM+ images from the USGS Landsat archive with a precision terrain correction L1T and covered by less than 70% clouds were considered (Griffiths et al., 2013a). Secondly, all images acquired within a two year range of the target years 1985, 1995 and 2010, and between mid-February and mid-November were retained. This range of acquisition months was included to avoid low sun elevation angles, shadowing and high snow coverage, but also allowed to maximize the amount of pixels in the final composite. The disadvantage of this large range of months (e.g., different phonological stages) was moreover minimized by inclusion of the day of year (DOY) in a parametric weighting scheme (see subsection “Pixel-based image compositing”).

Topographic correction was performed based on the co-registered 3 arc sec ($90 \text{ m} \times 90 \text{ m}$) digital elevation model (DEM). This space shuttle radar topography mission data (SRTM version 4.1; Slater et al., 2006) from CGIARCSI/NASA, which was resampled to the $30 \text{ m} \times 30 \text{ m}$ Landsat dataset by means of a bicubic spline interpolation. Although the resampled SRTM data do not allow an perfect topographic correction (e.g., Zhang et al. (2015) concluded that a 30 m DEM achieved the required topographic correction accuracy for $90\text{--}500 \text{ m}$ resolution remote sensing images), it is the best DEM available and it was preferred over the 1 arc sec ($30 \text{ m} \times 30 \text{ m}$) ASTER GDEM data as several studies indicate that the ASTER GDEM is more subject to artifacts such as stripes or cloud anomalies (Van Ede, 2004; Hirt et al., 2010).

Pixel-based image compositing

Griffiths et al. (2013b) implemented a PBIC algorithm to produce cloud-free and best observation composites of leaf-on phenology for a target year. Suitability of a given pixel was based on a parametric decision function which included: (1) the difference between acquisition year and target year, (2) the acquisition DOY, and (3)

the pixel's distance to the next cloud/shadow. For each pixel in each acquisition, scores across the parameters were combined. Based on these scores the best acquisition date was determined per pixel and all spectral band values of that best acquisition were written into the final best observation composite for the target year (Griffiths et al., 2013b).

Fig. 2 shows an illustration of the implemented PBIC procedure with 3 available input images, while in this study more than 1000 images were available for the three target years (i.e., 1985, 1995, 2010). In a first step (Fig. 2a), all footprints were (i) georeferenced, (ii) atmospherically corrected with the Landsat Ecosystem Disturbance Adaptive Processing System (LEDAPS) algorithm (Masek et al., 2006) and (iii) masked for clouds using the FMASK algorithm (Zhu and Woodcock, 2012). Secondly, a pixel-based composite was constructed for each target year by sampling the most suitable pixel for each cell from the all available imagery (Griffiths et al., 2013a; Fig. 2b).

During the suitability assessment, the most suitable observation for each cell was assessed based on three parameters, for which a pixel score was calculated (Griffiths et al., 2013a): acquisition year (i.e. annual suitability), DOY (i.e. seasonal suitability), and distance of a pixel to the most nearby cloud (i.e. risk of atmospheric disturbance). Highly suitable pixels have (i) an acquisition year close to target year, (ii) a DOY close to 183, which is an approximation of the period of main photosynthetic activity in Romania (Griffiths et al., 2013a), and (iii) no adjacent clouds. Afterwards, the total weighting of the pixel scores was obtained according to a flexible parametric weighting scheme (Griffiths et al., 2013a). In this weighting scheme, scores were calculated according to the year median DOY, preferred seasonal window and the distance to clouds. In this weighting scheme acquisitions within 30 days of the target DOY (i.e. May 28th and August 26th) are favored over images acquired one year before/after the target year, whereas acquisitions within a 45 day range of the target DOY are selected over images acquired two years from the target year. Finally, all scores are summed for each pixel in each acquisition and the most optimal acquisition (i.e. the highest final score) per pixel is selected. All six spectral bands for that pixel-acquisition combination were finally used to construct the PBIC that also contains the solar and illumination parameters (e.g. different incidence and zenith solar angles) of each pixel in separate bands (Griffiths et al., 2013a).

Pixel-based topographic correction of image composites

In this study, the PBIC procedure was applied on the total Landsat archive to generate three composites for target years 1985, 1995 and 2010. Additionally, an alternative composite was constructed by topographically correcting the pixel-based composite based on the pixel-based Minnaert (PBM) correction method of the ATCOR3 correction (Fig. 2c). ATCOR3 was first proposed by Richter (1998) and its PBM was shown to be the optimal topographic correction method for the Carpathian study region (Vanonckelen et al., 2014).

The PBM correction in the ATCOR3 method is based on a set of empirical rules (Richter et al., 2009). In a first step, the Lambertian or Cosine correction assumes a uniform reflectance of incident solar energy in all directions (Lu et al., 2008; Richter et al., 2009; Balthazar et al., 2012). The incident solar angle β is the angle between the normal to the ground surface and the solar zenith direction (Civco, 1989). The cosine of the incident solar angle is calculated with Eq. (1) and varies between -1 and +1:

$$\cos \beta = \cos \vartheta_s \cos \vartheta_n + \sin \vartheta_s \sin \vartheta_n \cos(\phi_t - \varphi_a) \quad (1)$$

where ϑ_n , ϕ_t and φ_a , are slope angle of the terrain, aspect angle of the terrain, and solar azimuth angle, respectively. In a second step, the normalized reflectance $\rho_{H,\lambda}$ is calculated with the correction parameter G which equals $(\cos \beta / \cos \beta_T)^b$ and where b is function of wavelength and vegetation cover, and β_T is a threshold value of

the incident solar angle β depending on the solar zenith angle ϑ_s (Eq. (2)):

$$\rho_{H,\lambda} = \rho_{T,\lambda} \left(\frac{\cos \beta}{\cos \beta_T} \right)^b \quad (2)$$

with b is function of the vegetation cover and wavelength. The PBM method of ATCOR3 combines two empirical parameters to calculate the bidirectional reflectance distribution function model: the lower boundary threshold of G and the threshold β_T (0–90°). The threshold of G regulates the intensity of the correction, whereas the threshold of β_T regulates the type of correction.

The lower boundary threshold of the factor G prevents an excessive reflectance reduction if the local solar zenith angle is substantially higher than the threshold angle (Richter and Schläpfer, 2013). Though a value of 0.25 is the standard threshold (Richter et al., 2009), an optimal lower boundary of 0.05 was derived in this study by examining the consistency between the reflectance values of opposite facing slopes and the resulting color composites using the method of Vanonckelen et al. (2014). Based on the 0.05 threshold overcorrection problems were removed in the natural and false color composites, as results shown in “Forest cover map” section.

The threshold β_T determines the type of correction, where β_T depends on ϑ_s plus an increment that according to its initial value (Richter et al., 2009):

$$\beta_T = \vartheta_s + 20^\circ \text{ if } \vartheta_s < 45^\circ \quad (3)$$

$$\beta_T = \vartheta_s + 15^\circ \text{ if } 45^\circ < \vartheta_s < 55^\circ \quad (4)$$

$$\beta_T = \vartheta_s + 10^\circ \text{ if } \vartheta_s > 55^\circ \quad (5)$$

When $\beta < \beta_T$, Lambertian correction is applied ($\rho_{H,\lambda} = \rho_{T,\lambda}$), whereas the corrected surface reflectance is converted according to Richter and Schläpfer (2013) when β exceeds β_T using:

$b = 1/2$ for non-vegetation;

$b = 3/4$ for vegetation in the visible spectrum ($\lambda < 720$ nm);

$b = 1/3$ for vegetation if $\lambda \geq 720$ nm.

The differentiation between vegetation and non-vegetation was based on the pixel-based NDVI value of 0.7 (normalized difference vegetation index), which basically corresponds to the difference between the forest classes (i.e. the dominant vegetation cover) and the non-forest class. This threshold value was determined by examining the natural and false color composites of five known study areas (each of about 500 km²) in combination with field knowledge and existing vegetation maps. Moreover, the dominant land cover type in the study area was vegetation.

$$NDVI = \frac{\rho_{NIR} - \rho_{red}}{\rho_{NIR} + \rho_{red}} \quad (6)$$

where ρ_{red} and ρ_{NIR} are reflectance measurements in % for the red and NIR bands. Fig. 3a and b is an illustration of the effect of topographic correction and show the true color composites without and with topographic correction of a detail of the study area. The difference in illumination is clearly visible in the composite without correction in Fig. 3a. However, the differential illumination effects are reduced in the topographically corrected Fig. 3b: equal forest cover types have comparable spectral values for similar terrain features on opposite facing slopes.

Forest cover classification

Based on the generated composites, large scale forest cover maps were compiled for the three target years using the Maximum Likelihood (ML) and Support Vector Machine (SVM) classifiers. The supervised ML classifier is based on the Gaussian distribution of the elements in the coherent scattering matrix (Foody, 2002). It is still

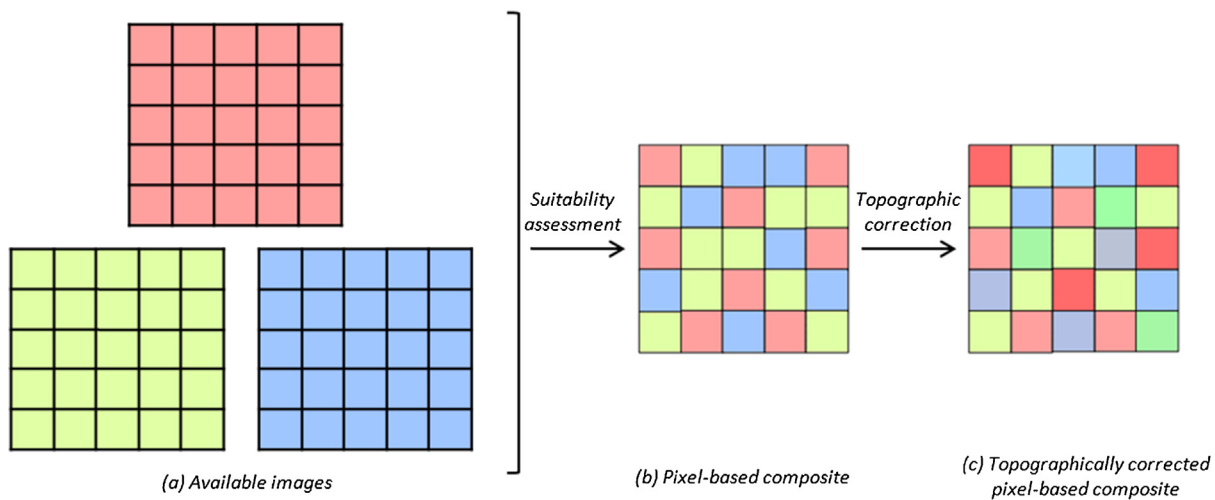


Fig. 2. Pixel-based compositing with (a) selection of all available images (in this example there are only 3 images available), (b) construction of the pixel-based composite with selection of the best pixel for each cell after a suitability assessment, and (c) topographically corrected pixel-based composite.

widely used as a supervised classification method ([Chen et al., 2004](#); [Mountrakis et al., 2011](#)) due to its convenient use when sufficient GCPs are available ([Gao and Zhang, 2009](#)).

The basic principle of a SVM classifier is to identify a hyperplane that optimally separates two classes in the feature space. The hyperplane is constructed in an iterative way by maximizing the distance among class boundaries (Foody et al., 2007; Alcantara et al., 2012). SVMs frequently outperform other non-parametric and parametric classifiers (Foody and Mathur, 2004) while requiring few training data (Huang et al., 2002; Pal and Mather, 2005; Guo et al., 2005; Dixon and Candade, 2008; Knorn et al., 2009). SVMs have been successfully applied to map forest cover changes over large areas (Huang et al., 2008; Kuemmerle et al., 2008; Sieber et al., 2013) and is well suited to map spectrally complex classes, such as in forest change analysis (Vapnik, 1999; Melgani and Bruzzone, 2004; Huang et al., 2008).

The ML and SVM classifier were implemented using ENVI/IDL and the EnMAP Box software ([van der Linden et al., 2010](#)) to differentiate 4 classes ([Table 1](#)): non-forest, broadleaved forest, mixed forest, and coniferous forest. As the focus of this study was to detect forest cover changes, all non-forest classes were grouped. A similar separation of classes was performed by [Olofsson et al. \(2011\)](#), [Griffiths et al. \(2013b\)](#) and [Main-Knorn et al. \(2013\)](#).

The ML and SVM classifiers of 2010 were trained based on randomly stratified points that were sampled using high resolution

imagery from Google Earth. For each forest cover class, a minimum of 900 training points was sampled (randomly stratified based on Google Earth interpretation) with a minimum distance of 1 km between adjacent points to minimize spatial autocorrelation (Campbell, 1981; Labovitz and Masuoka, 1984; Table 1). Since reference data were unavailable for 1985 and 1995, the 2010 training data were selected and verified on the 1985 and 1995 pixel-based composites. Validation was performed with a different set of sample points that were sampled independently based on randomly sampled GCP points from two sources: fieldwork and high-resolution WorldView-2 imagery: (1) GCP-collection during field visits in May 2010 and July 2011; and (2) GCP-identification on high-resolution satellite imagery (WorldView-2, 8 bands, 46 cm resolution, acquisition date October 13, 2010). The selection of the samples was equal for both topographic and non-topographic correction.

Evaluation of forest cover classification

Evaluation of the results consisted of assessing overall accuracy (OA) and forest cover specific producer's and user's accuracies ([Congalton, 1991](#); [Foody, 2002](#)) for four different scenarios:

- (1) ML with 4 classes—topographically uncorrected;
 - (2) ML with 4 classes—topographically corrected;
 - (3) SVM with 4 classes—topographically uncorrected;

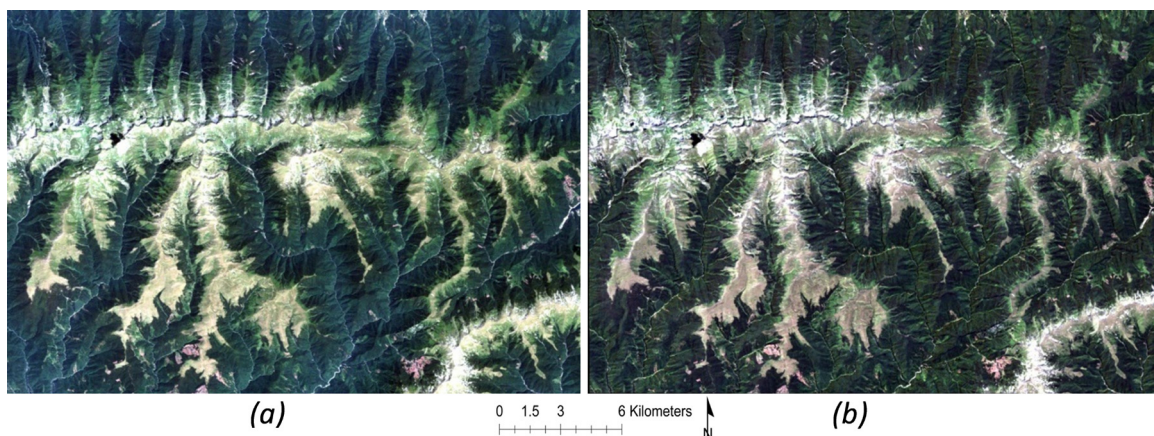


Fig. 3. Detail of the study area with (a) true color composite (RGB: band 3, 2 and 1) without topographic correction, and (b) true color composite with topographic correction.

Table 1

Forest cover classes, code, dominant species and average training and test samples of 2010, 1995 and 1985 (separated by slashes) in the study area.

Forest cover classes	Code	Dominant species	Average training samples	Average test samples
Broadleaved forest	BL	<i>Carpinus betulus</i> , <i>Fagus sylvatica</i> , <i>Quercus petraea</i> , <i>Quercus robur</i>	900/875/850	100/90/85
Coniferous forest	CF	<i>Abies alba</i> , <i>Picea abies</i> , <i>Pinus mugo</i> , <i>Pinus sylvestris</i>	900/850/810	100/90/85
Mixed forest	MX	Mixture of the dominant BL and CF forest species	900/875/850	100/90/85
Non-forest	NF	–	2000/1850/1700	200/180/165

Non-forest (NF), broadleaved (BL), coniferous (CF) and mixed forest (MX). Mixed forests are stands where neither broadleaved nor coniferous trees account for more than 75% of the tree crown area (UN-ECE/FAO, 2000).

Table 2

Classification accuracy assessment of a topographically uncorrected Maximum Likelihood classification of 1985, 1995 and 2010 (separated by commas and in %).

Reference	Classification											
	NF			BL			MX			CF		
	1985	1995	2010	1985	1995	2010	1985	1995	2010	1985	1995	2010
NF	77	78	88	10	4	7	6	7	3	3	6	4
BL	8	6	10	79	92	82	9	8	6	2	2	5
MX	5	6	2	4	4	8	63	62	79	3	12	12
CF	7	11	4	7	2	2	20	24	11	84	82	81
PA	77	78	88	79	92	82	63	62	79	84	82	81
UA	87	89	85	70	79	79	53	57	75	58	72	69
OA											78	79
												84

Non-forest (NF), broadleaved forest (BL), coniferous forest (CF) and mixed forest (MX). Producer's Accuracy (PA), User's Accuracy (UA) and Overall Accuracy (OA). Note: accuracy values are provided as integers, consequently it is possible that the sum over all forest cover classes is not exactly 100.

(4) SVM with 4 classes—topographically corrected.

Results

Forest cover accuracies

An overview of the classification accuracy of the ML classification without (Table 2) and with (Table 3) topographical correction for the different target years is presented in Tables 2 and 3. The produced forest cover maps based on the topographically uncorrected data have overall accuracy values of 78% (1985), 79% (1995) and 84% (2010) with highest accuracies for the CF and BL classes (i.e. producer's accuracy between 81–84% for CF and 79–92% for BL respectively). The MX class shows lower accuracies (i.e. producer's accuracies between 62% and 79%), which can be explained by the mixed nature of this class that makes it more difficult to classify. Comparison of Tables 2 and 3 indicates that topographic correction results in a small increase in overall accuracy for the ML classifier with respectively 3% (1985), 3% (1995) and 2% (2010).

Tables 4 and 5 illustrate the classification accuracy when applying SVM without (Table 4) and with (Table 5) topographical correction. Comparison of the classifiers without topographical correction (ML in Table 2 vs. SVM in Table 4) shows that applying an improved classifier results in higher overall and class accuracies.

For example, the OA increases by 5% (1985), 4% (1995) and 5% (2010), whereas the producer's accuracies of MX increase by 7% (1985), 5% (1995) and 6% (2010). Similar effects can be seen when comparing ML and SVM for topographically corrected data (ML in Table 3 vs. SVM in Table 5) as switching to SVM results in increases in overall classification accuracies of 4% (1985), 1% (1995) and 5% (2010), respectively, whereas the producer's accuracy increase by 5% (1985), 1% (1995) and 3% (2010) for the CF forest class and by 4% (1985), 0% (1995) and 4% (2010) for the MX forest class.

The classification accuracies of the uncorrected classified composites (Tables 2 and 4) are lower than the accuracies of the corrected classified composites (Tables 3 and 5). This is shown by overall accuracy increases of respectively 3%, 3% and 2% between Tables 2 and 4 (ML scenario), and respectively 2%, 0% and 2% between Tables 3 and 5 (SVM scenario). In this study, the impact of the topographic correction on classification accuracy is smaller than the impact of the classifier.

Forest cover maps

The previous section demonstrated that the highest classification accuracies were achieved by the topographically corrected SVM composites. Therefore, the resulting forest cover maps with the highest overall accuracies – the topographically corrected SVM

Table 3

Classification accuracy assessment of a topographically corrected Maximum Likelihood classification of 1985, 1995 and 2010 (separated by commas and in %).

Reference	Classification											
	NF			BL			MX			CF		
	1985	1995	2010	1985	1995	2010	1985	1995	2010	1985	1995	2010
NF	80	80	91	10	3	6	5	6	2	2	5	2
BL	7	5	7	81	96	86	9	7	5	2	2	3
MX	4	6	3	3	2	6	68	82	5	10	11	11
CF	6	9	3	6	1	2	18	22	10	87	85	85
PA	80	80	91	81	96	86	68	66	82	87	85	85
UA	91	92	88	73	83	81	56	60	77	61	76	71
OA											81	82
												86

Non-forest (NF), broadleaved forest (BL), coniferous forest (CF) and mixed forest (MX). Producer's Accuracy (PA), User's Accuracy (UA) and Overall Accuracy (OA). Note: accuracy values are provided as integers, consequently it is possible that the sum over all forest cover classes is not exactly 100.

Table 4

Classification accuracy assessment of a topographically uncorrected Support Vector Machine classification of 1985, 1995 and 2010 (separated by commas and in %).

Reference	Classification											
	NF			BL			MX			CF		
	1985	1995	2010	1985	1995	2010	1985	1995	2010	1985	1995	2010
NF	82	81	94	8	2	4	5	5	1	1	4	1
BL	7	6	7	84	97	89	8	6	4	1	1	3
MX	3	6	2	2	1	5	70	67	85	5	10	10
CF	5	7	1	5	0	1	17	23	9	89	86	87
PA	82	81	94	84	97	89	70	67	85	89	86	87
UA	93	94	90	75	85	83	57	61	80	63	78	74
OA										83	83	89

Non-forest (NF), broadleaved forest (BL), coniferous forest (CF) and mixed forest (MX). Producer's Accuracy (PA), User's Accuracy (UA) and Overall Accuracy (OA). Note: accuracy values are provided as integers, consequently it is possible that the sum over all forest cover classes is not exactly 100.

Table 5

Classification accuracy assessment of a topographically corrected Support Vector Machine classification of 1985, 1995 and 2010 (separated by commas and in %).

Reference	Classification											
	NF			BL			MX			CF		
	1985	1995	2010	1985	1995	2010	1985	1995	2010	1985	1995	2010
NF	85	83	97	7	1	2	5	5	1	1	4	1
BL	5	5	1	85	97	89	6	5	4	0	1	1
MX	3	5	1	1	2	8	72	66	86	6	10	11
CF	4	6	1	6	0	1	17	25	10	92	86	88
PA	85	83	97	85	97	89	72	66	86	92	86	88
UA	98	96	93	76	85	84	59	62	81	64	77	75
OA										85	83	91

Non-forest (NF), broadleaved forest (BL), coniferous forest (CF) and mixed forest (MX). Producer's Accuracy (PA), User's Accuracy (UA) and Overall Accuracy (OA). Note: accuracy values are provided as integers, consequently it is possible that the sum over all forest cover classes is not exactly 100.

composites – are presented in Fig. 4a–c. Fig. 4a presents the forest cover map of the Romanian Carpathians in 1985. The Romanian Carpathian mountain range is dominated by the forest classes, with broadleaved forest in light green, coniferous forest in dark green and mixed forest in between. Lower elevated areas – located in the center and northwest corner of the map – are dominated by the non-forest class, especially arable land and grassland. In general, no major changes are present in the three figures. However, it is possible to discern a gradual greening of some areas in 1995 (Fig. 4b) and 2010 (Fig. 4c). In order to support the visual results, the statistics of the forest cover types were calculated and presented.

Fig. 5 shows the statistics in percentage of the topographically corrected SVM classification in the Romanian Carpathian Ecoregion. The general trends between 1985 and 2010 show a decrease of $\pm 5\%$ in the non-forest class and consequently a similar increase in the forest class. In 1985, the forest cover map consisted for 57% of NF, 27% of BL, 10% of MX and 7% of CF. Compared to 1985,

Fig. 5 denotes an increase in the BL and MX forest cover classes in 1995 and 2010. The CF forest class remains stable. The increase from 10% to 13% between 1985 and 2010 was largest in the mixed forest class, followed by an increase from 27% to 29% in the similar period for the BL class. In contrast, CF forest remained stable between 1985 and 2010, with a minor increase between 1985 and 1995.

In Table 6, these statistics are also summarized in ha for the Romanian Carpathian Ecoregion. The non-forest class accounts for more than half of the surface area, followed by the BL, MX and CF class. The decrease in the non-forest class between 1985 and 2010 ($-516,072$ ha) is especially compensated by an increase in the BL and MX forest classes with respectively increases of 302,784 ha and 217,162 ha. The CF forest class experienced a small decline of 3874 ha between 1985 and 2010. Table 6 also shows that the total forest area increased from $\pm 4,614,864$ ha in 1985 to $\pm 5,130,936$ ha in 2010.

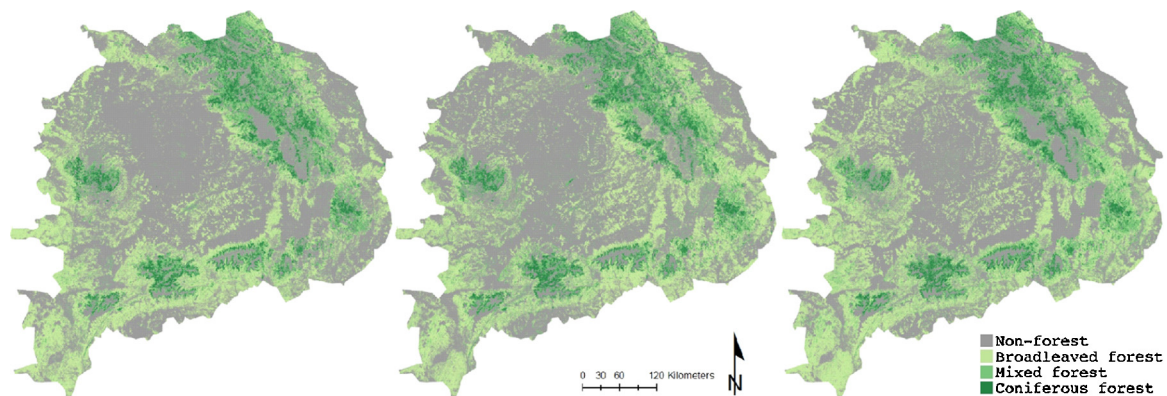


Fig. 4. Forest cover maps in the Romanian Carpathian Ecoregion of the topographically corrected SVM composites of (a) 1985, (b) 1995 and (c) 2010.

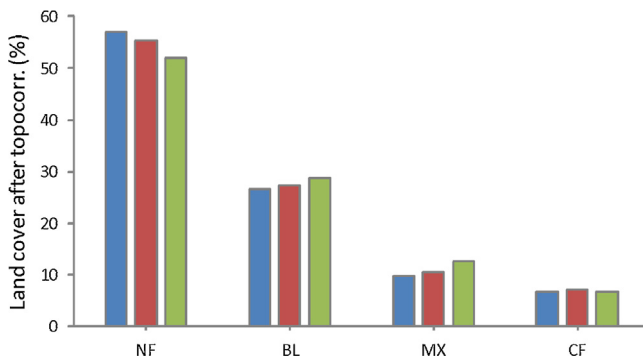


Fig. 5. Statistics of the topographically corrected SVM composites of 1985, 1995 and 2010 in the Romanian Carpathian Ecoregion. The average standard deviation over all forest cover types and bands for the 3 years was respectively 1.85 for 1985, 1.64 for 1995 and 1.38 for 2010. Non-forest (NF), and broadleaved (BL), mixed (MX) and coniferous (CF) and forest.

Table 6
Forest cover area in ha of the 4 forest cover classes of 1985, 1995 and 2010.

Forest cover area (ha)	1985	1995	2010
NF	6,100,236	5,927,443	5,584,164
BL	2,859,076	2,920,346	3,076,238
MX	1,034,334	1,111,709	1,337,118
CF	721,453	755,602	717,579
Total forest	4,614,864	4,787,657	5,130,936

Broadleaved forest (BL), mixed forest (MX), coniferous forest (CF) and non-forest (NF).

Discussion

Hitherto, forest cover dynamics in the Romanian Carpathians were described by means of local scale case studies and topographically corrected Landsat composites were missing at regional scale. In this study, classification accuracies were assessed for four different scenarios in which 2 components were altered: classifier (ML or SVM) and topographic correction (uncorrected or corrected).

The effect of topographic correction on PBIC

The overall accuracy of the forest cover maps produced in this study were higher than a similar large scale study of Griffiths et al. (2013a) which obtained an OA of 65% on the pixel-based image composites without topographic correction using a random forest classifier. Furthermore, UA values were ranging between 9% and 94%, and PA values varied between 36% and 96%. Another local scale study on one multi-temporal Landsat TM footprint in Oregon by Kennedy et al. (2007) selected the most suitable pixels based on the temporal signatures of spectral values that are associated with different forest cover changes. Here, the automated method labeled the year of disturbance with 90% overall accuracy in clear-cuts and with 77% accuracy in partial-cuts.

Forest cover mapping in the Romanian Carpathian Ecoregion

Since large (virgin) forests are located in mountain environments, the methodology and results of this study can be implemented in further analyses to improve the detection of forest cover change. As documented in this study, the selection of an appropriate classifier is even more important than a topographic correction. However, a similar analysis should be conducted in a study area with extreme topography.

Generally, the main forest cover conversion between 1985–1995 and 1995–2010 was the conversion of non-forest in forest. A steady greening of the Romanian Carpathian Ecoregion

was observed since afforestation was larger than deforestation in the two periods. Between 1985 and 2010, a decrease of $\pm 5\%$ in the non-forest class was compensated by an increase in the forest class (Table 6). The decrease in the non-forest class between 1985 and 2010 ($-516,072$ ha) was especially compensated by an increase in the BL and MX forest classes with respectively increases of $\pm 302,784$ ha and $\pm 217,162$ ha. The CF forest class experienced a small decline of $\pm 3,874$ ha between 1985 and 2010. Table 6 also showed that the total forest area increased from $\pm 4,614,864$ ha in 1985 to $\pm 5,130,936$ ha in 2010. Griffiths et al. (2013b) examined forest disturbances across the Romanian Carpathian Ecoregion, based on a SVM classification of topographically uncorrected images. Results showed that large changes in forest composition between 1985 and 2010 occurred in Romania: coniferous forests decreased with 7% or $\pm 197,330$ ha between 1985 and 2010, while broadleaved and mixed forests increased with 12% and 2% or respectively $\pm 1,095,030$ ha and $\pm 233,290$ ha (Griffiths et al., 2013b). In general, the total forest area increased from $\pm 6,027,370$ ha in 1985 to $\pm 7,158,360$ ha in 2010. Moreover, the Global Forest Resources Assessment of FAO (2010) reported $\pm 6,573,000$ ha of Romanian forest area in 2010. Based on this comparison, our results reflect conservative estimates of forest cover and forest cover change.

Since only one optimal pixel near the median DOY of 183 was selected for each year, phenology-related errors due to missing effects of crop cycles were included in the analysis. In a comparable analysis of Griffiths et al. (2012) on one Romanian Landsat footprint, the acquisition dates of some images between mid-October and late-May explained lower accuracies due to strong phenology and illumination differences. Therefore, future versions of the PBIC algorithm should address the potential of different phenology measures by including specific temporal and spectral observations (Griffiths et al., 2012). The decision for image selection during pixel-based compositing procedure was based on a flexible parametric weighting scheme that evaluated available observations for their suitability. However, this decision system lacks a parameter that quantifies the atmospheric or topographic distortion. For example, the observation with the lowest reflectance in the blue band can be selected to minimize the atmospheric effects (Griffiths et al., 2013a). Finally, the determination of the optimal lower boundary threshold of the correction parameter G can be improved, e.g. by an optimization procedure such as performed by Balthazar et al. (2012).

Conclusion

So far, several multi-temporal analyses were performed with mosaicked satellite data or with pixel-based image composites. However, at present, the inclusion of a topographic correction in the compositing of Landsat data was still lacking. In this study, a topographic correction was included in the pixel-based image compositing algorithm and tested between 1985 and 2010. The multi-temporal analysis in the Romanian Carpathian Ecoregion provided large scale topographically corrected maps and accuracy results. In this context, the classification accuracy was assessed for four different scenarios in which 2 components were altered: classifier (ML or SVM) and topographic correction (uncorrected or corrected).

Forest cover accuracies were assessed and compared for the four scenarios. The topographically uncorrected ML classification for 4 forest cover classes resulted in overall accuracies of respectively of 78% (1985), 79% (1995) and 84% (2010). The topographic correction improved the ML classification with respectively 3% (1985), 3% (1995) and 2% (2010). The SVM classification was also performed on the topographically uncorrected and corrected composites. The

topographically uncorrected SVM classification obtained overall accuracies of respectively 83% (1985), 83% (1995) and 89% (2010). The corrected SVM classification resulted in overall classification accuracies increases of respectively 2% (1985), 0% (1995) and 2% (2010). Generally, the overall accuracies for 4 forest cover classes was between 78% and 91% for all years. The overall accuracy values were highest for the forest cover maps of 2010.

Moreover, the results indicated that the implementation of a topographic correction had a smaller influence on the classification accuracies than the selection of a classifier. This was shown by a larger increase in classification accuracy after conversion from ML to SVM classifier than after conversion from the uncorrected to the corrected scenarios. The overall classification accuracies of the best scenario – the topographically corrected SVM classification – were respectively 85% (1985), 83% (1995) and 91% (2010). A steady greening of the Romanian Carpathian Ecoregion was observed between 1985 and 2010 since afforestation was larger than deforestation. Between 1985 and 2010, a decrease of $\pm 5\%$ in the non-forest class was compensated by an increase in the forest class. This decrease in the non-forest class was especially compensated by an increase in the broadleaved and mixed forest classes.

The further development of automatic detection methods based on time series with a high temporal resolution is helpful for the identification of forest cover changes. In a following step, the application of topographic correction before the pixel-based image compositing deserves further elaboration. This application would allow the inclusion of a parameter that quantifies the illumination effects and improves the input map for classification. Especially change detection studies in mountain areas could profit from such improvements.

Acknowledgements

This research was funded by the Belgian Science Policy, Research Program for Earth Observation Stereo II, contract SR/00/133, as part of the FOMO project (remote sensing of the forest transition and its ecosystem impacts in mountain environments). The research was carried out in collaboration with Prof. Patrick Hostert and Dr. Patrick Griffiths from the Geography Department at the Humboldt-University in Berlin. Stef Lhermitte was supported as postdoctoral researcher by Fonds Wetenschappelijk Onderzoek – Vlaanderen.

References

- Alcantara, C., Radeloff, V.C., Prishchepov, A.V., Kuemmerle, T., 2012. Mapping abandoned agriculture with multi-temporal MODIS satellite data. *Remote Sens. Environ.* 124, 334–347.
- Arvidson, T., Gasch, J., Goward, S.N., 2001. Landsat 7's long term acquisition plan—an innovative approach to building a global archive. Special Issue on Landsat 7. *Remote Sens. Environ.* 78, 13–26.
- Arvidson, T., Goward, S., Gasch, J., Williams, D., 2006. Landsat-7 long-term acquisition plan: development and validation. *Photogram. Eng. Remote Sens.* 72, 1137–1146.
- Balthazar, V., Vanacker, V., Lambin, E., 2012. Evaluation and parameterization of ATCOR3 topographic correction method for forest cover mapping in mountain areas. *Int. J. Appl. Earth Obs. Geoinform.* 18, 436–450.
- Berk, A., Bernstein, L.S., Anderson, G.P., Robertson, D.C., Chetwynd, J.H., Adler-Golden, S.M., 1998. MODTRAN cloud and multiple scattering upgrades with application to AVIRIS. *Remote Sens. Environ.* 65, 367–375.
- Broich, M., Hansen, M.C., Potapov, P., Adusei, B., Lindquist, E., Stehman, S.V., 2011. Time-series analysis of multi-resolution optical imagery for quantifying forest cover loss in Sumatra and Kalimantan, Indonesia. *Int. J. Appl. Earth Obs. Geoinform.* 13, 277–291.
- Campbell, J.B., 1981. Spatial correlation effects upon accuracy of supervised classification of forest cover. *Photogram. Eng. Remote Sens.* 47, 355–363.
- Chen, D., Stow, D.A., Gong, P., 2004. Examining the effect of spatial resolution and texture window size on classification accuracy: an urban environment case. *Int. J. Remote Sens.* 25, 2177–2192.
- Cihlar, J., Manak, D., Diorio, M., 1994. Evaluation of compositing algorithms for AVHRR data over land. *IEEE Trans. Geosci. Remote Sens.* 32, 427–437.
- Civco, D.L., 1989. Topographic normalization of Landsat Thematic Mapper digital imagery. *Photogram. Eng. Remote Sens.* 55, 1303–1309.
- Congalton, R.G., 1991. A review of assessing the accuracy of classifications of remotely sensed data. *Remote Sens. Environ.* 37, 35–46.
- Dixon, B., Candade, N., 2008. Multispectral land use classification using neural networks and support vector machines: One or the other, or both? *Int. J. Remote Sens.* 29, 1185–1206.
- FAO/UNESCO/WRB, 146 pp. 1998. Soil Map of the World, Revised Legend. *World Soil Resources Report 60*, Rome.
- FAO, 2010. Global Forest Resources Assessment 2010. Rome, Italy., 340 pp.
- FAO, 2012. Global Forest Land-Use Change 1990–2005. FAO Forestry Paper No. 169, Rome.
- Foley, J.A., DeFries, R., Asner, G.P., Barford, C., Bonan, G., Carpenter, S.R., Chapin, F.S., Coe, M.T., Daily, G.C., Gibbs, H.K., Helkowski, J.H., Holloway, T., Howard, E.A., Kucharik, C.J., Monfreda, C., Patz, J.A., Prentice, I.C., Ramankutty, N., Snyder, P.K., 2005. Global consequences of land use. *Science* 309, 570–574.
- Foody, G.M., 2002. Status of forest cover classification accuracy assessment. *Remote Sens. Environ.* 80, 185–201.
- Foody, G.M., Mathur, A., 2004. Toward intelligent training of supervised image classifications: directing training data acquisition for SVM classification. *Remote Sens. Environ.* 93, 107–117.
- Foody, G.M., Boyd, D.S., Sanchez-Hernandez, C., 2007. Mapping a specific class with an ensemble of classifiers. *Int. J. Remote Sens.* 28, 1733–1746.
- Gao, Y., Zhang, W., 2009. LULC classification and topographic correction of landsat-7 ETM+ Imagery in the Yangtze River watershed: the influence of DEM resolution. *Sensors* 9, 1980–1995.
- Giri, C., Pengra, B., Long, J., Loveland, T.R., 2013. Next generation of global forest cover characterization, mapping, and monitoring. *Int. J. Appl. Earth Obs. Geoinform.* 25, 30–37.
- Goward, S.N., Haskett, J., Williams, D., Arvidson, T., Gasch, J., Lonigro, R., Reely, M., Irons, J., Dubayah, R., Turner, S., Campana, K., Bindschadler, R., 1999. Enhanced Landsat capturing all the Earth's land areas. *EOS* 80 (26), 289–293.
- Griffiths, P., Kuemmerle, T., Kennedy, R.E., Abrudan, I.V., Knorn, J., Hostert, P., 2012. Using annual time-series of Landsat images to assess the effects of forest restitution in post-socialist Romania. *Remote Sens. Environ.* 118, 199–214.
- Griffiths, P., van der Linden, S., Kuemmerle, T., Hostert, P., 2013a. A pixel-based landsat compositing algorithm for large area forest cover mapping. *IEEE J. Select. Top. Appl. Earth Obs. Remote Sens.*, 1–14.
- Griffiths, P., Kuemmerle, T., Baumann, M., Radeloff, V.C., Abrudan, I.V., Lieskovsky, J., Munteanu, C., Ostapowicz, K., Hostert, P., 2013b. Forest disturbances, forest recovery, and changes in forest types across the Carpathian ecoregion from 1985 to 2010 based on Landsat image composites. *Remote Sens. Environ.*, <http://dx.doi.org/10.1016/j.rse.2013.04.022>.
- Guo, Q., Kelly, M., Graham, C.H., 2005. Support vector machines for predicting distribution of Sudden Oak Death in California. *Ecol. Modell.* 182, 75–90.
- Hansen, M.C., DeFries, R.S., 2004. Land use change and biodiversity. *Ecosystems* 7, 695–716.
- Hansen, M.C., Roy, D.P., Lindquist, E., Adusei, B., Justice, C.O., Altstatt, A., 2008. A method for integrating MODIS and Landsat data for systematic monitoring of forest cover and change in the Congo Basin. *Remote Sens. Environ.* 112, 2495–2513.
- Hansen, M.C., Egorov, A., Roy, D.P., Potapov, P., Ju, J., Turubanova, S., Kommareddy, I., Loveland, T.R., 2011. Continuous fields of forest cover for the conterminous United States using Landsat data: first results from the Web-Enabled Landsat Data (WELD) project. *Remote Sens. Lett.* 2, 279–288.
- Hansen, M.C., Potapov, P.V., Moore, R., Hanch, M., Turubanova, S.A., Tyukavina, A., Thau, D., Stehman, S.V., Goetz, S.J., Loveland, T.R., Kommareddy, A., Egorov, A., Chini, L., Justice, C.O., Townshend, J.R.G., 2013. High-resolution global maps of 21st-century forest cover change. *Science* 342 (6160), 850–853.
- Hirt, C., Filmer, M.S., Featherstone, W.E., 2010. Comparison and validation of the recent freely-available ASTER GDEM ver1, SRTM ver4.1 and GEODATA DEM-9S ver3 digital elevation models over Australia. *Austr. J. Earth Sci.* 57, 337–347.
- Holben, B.N., 1986. Characteristics of maximum-value composite images from temporal AVHRR data. *Int. J. Remote Sens.* 7, 1417–1434.
- Huang, C., Davis, L.S., Townshend, J.R.G., 2002. An assessment of support vector machines for forest cover classification. *Int. J. Remote Sens.* 23, 725–749.
- Huang, H., Gong, P., Clinton, N., Hui, F., 2008. Reduction of atmospheric and topographic effect on Landsat TM data for forest classification. *Int. J. Remote Sens.* 29, 5623–5642.
- Jensen, J.R., 1996. *Introduction Digital Image Processing: A Remote Sensing Perspective*, third ed. Prentice-Hall, Englewood Cliffs, NJ.
- Ju, J., Roy, D.P., 2008. The availability of cloud-free Landsat ETM plus data over the conterminous United States and globally. *Remote Sens. Environ.* 112, 1196–1211.
- Kennedy, R.E., Cohen, W.B., Schroeder, T.A., 2007. Trajectory-based change detection for automated characterization of forest disturbance dynamics. *Remote Sens. Environ.* 110, 370–386.
- Kennedy, R.E., Yang, Z., Cohen, W.B., 2010. Detecting trends in forest disturbance and recovery using yearly Landsat time series: 1. LandTrendr - temporal segmentation algorithms. *Remote Sens. Environ.* 114, 2897–2910.
- Knorn, J., Rabe, A., Radeloff, V.C., Kuemmerle, T., Kozak, J., Hostert, P., 2009. Forest cover mapping of large areas using chain classification of neighboring Landsat satellite images. *Remote Sens. Environ.* 113, 957–964.
- Kuemmerle, T., Hostert, P., Radeloff, V.C., van der Linden, S., Perzanowski, K., Kruehl, I., 2008. Cross-border comparison of post-socialist farmland abandonment in the Carpathians. *Ecosystems* 11, 614–628.

- Labovitz, M.L., Masuoka, E.J., 1984. The influence of autocorrelation in signature extraction: an example from a geobotanical investigation of Cotter Basin, Montana. *Int. J. Remote Sens.* 5, 315–332.
- Lambin, E.F., Geist, H.J., 2006. Land Use and Forest cover Change, Local Processes and Global Impacts, third ed. Springer-Verlag, Heidelberg/Berlin/New York.
- Lhermitte, S., Verbesselt, J., Verstraeten, W.W., Coppin, P., 2011a. A comparison of time series similarity measures for classification and change detection of ecosystem dynamics. *Remote Sens. Environ.* 115, 3129–3152.
- Lhermitte, S., Verbesselt, J., Verstraeten, W.W., Veraverbeke, S., Coppin, P., 2011b. Assessing intra-annual vegetation regrowth after fire using the pixel based regeneration index. *ISPRS J. Photogram. Rem. Sens.* 66, 17–27.
- Loveland, T.R., Dwyer, J.L., 2012. Landsat: building a strong future. *Remote Sens. Environ.* 122, 22–29.
- Lu, D., Ge, H., He, S., Xu, A., Zhou, G., Du, H., 2008. Pixel-based Minnaert correction method for reducing topographic effects on a Landsat-7 ETM+ image. *Photogram. Eng. Remote Sens.* 74, 1343–1350.
- Main-Knorn, M., Cohen, W.B., Kennedy, R.E., Grodzki, W., Pflugmacher, D., Griffiths, P., Hostert, P., 2013. Monitoring coniferous forest biomass change using a Landsat trajectory-based approach. *Remote Sens. Environ.* 139, 277–290.
- Masek, J.G., Vermote, E.F., Saleous, N.E., Wolfe, R., Hall, F.G., Huemmrich, K.F., Gao, F., Kutler, J., Lim, T.K., 2006. A Landsat surface reflectance dataset for North America, 1990–2000. *IEEE Geosci. Remote Sens. Lett.* 3, 68–72.
- Melgani, F., Bruzzone, L., 2004. Classification of hyperspectral remote sensing images with support vector machines. *IEEE Trans. Geosci. Remote Sens.* 42, 1778–1790.
- Meyer, P., Itten, K.I., Kellenberger, T., Sandmeier, S., Sandmeier, R., 1993. Radiometric corrections of topographically induced effects on Landsat TM data in alpine environment. *J. Photogr. Remote Sens.* 48, 17–28.
- Meyfroidt, P., Lambin, E.F., 2011. Global forest transition: prospects for an end to deforestation. *Annu. Rev. Environ. Resour.* 36, 343–371.
- Mihai, B., Savulescu, I., Sandric, I., 2007. Change detection analysis (1986–2002) of vegetation cover in Romania: a study of alpine, subalpine, and forest landscapes in the Lezern mountains. *Southern Carpathians Mount. Res. Develop.* 27, 250–258.
- Millennium Development Goals Report, 2013. United Nations, June 2013. New York, 68 pp.
- Minnaert, N., 1941. The reciprocity principle in lunar photometry. *Astrophys. J.* 93, 403–410.
- Mountakis, G., Im, J., Ogole, C., 2011. Support vector machines in remote sensing: a review. *ISPRS. J. Photogr. Remote Sens.* 66 (3), 247–259.
- Müller, D., Kuemmerle, T., Rusu, M., Griffiths, P., 2009. Lost in transition: determinants of post-socialist cropland abandonment in Romania. *J. Land Use Sci.* 4 (1–2), 109–129.
- Olofsson, P., Kuemmerle, T., Griffiths, P., Knorn, J., Baccini, A., Gancz, V., Blujdea, V., Houghton, R.A., Abrudan, I.V., Woodcock, C., 2011. Carbon implications of forest restitution in post-socialist Romania. *Environ. Res. Lett.* 6, 1–10.
- Pal, M., Mather, P.M., 2005. Support vector machines for classification in remote sensing. *Int. J. Remote Sens.* 26, 1007–1011.
- Potapov, P.V., Turubanova, S.A., Hansen, M.C., 2011. Regional-scale boreal forest cover and change mapping using Landsat data composites for European Russia. *Remote Sens. Environ.* 115, 548–561.
- Potapov, P.V., Turubanova, S.A., Hansen, M.C., Adusei, B., Broich, M., Altstatt, A., Mane, L., Justice, C.O., 2012. Quantifying forest cover loss in Democratic Republic of the Congo, 2000–2010, with Landsat ETM+ data. *Remote Sens. Environ.* 122, 106–116.
- Riano, D., Chuvieco, E., Salas, F.J., Aguado, I., 2003. Assessment of different topographic corrections in Landsat TM data for mapping vegetation types. *IEEE Trans. Geosci. Remote Sens.* 41, 1056–1061.
- Richter, R., 1996. Atmospheric correction of satellite data with haze removal including a haze/clear transition region. *Comp. Geosci.* 2, 675–681.
- Richter, R., 1998. Correction of satellite imagery over mountainous terrain. *Appl. Opt.* 37, 4004–4015.
- Richter, R., Kellenberger, T., Kaufmann, H., 2009. Comparison of topographic correction methods. *Remote Sens.* 1, 184–196.
- Richter, R., Schläpfer, D., 2013. Atmospheric/Topographic Correction for Satellite Imagery. Atcor-2/3 User Guide, version 8.2.1, February 2013. Available at <http://www.rese.ch/pdf/atcor3.manual.pdf> (Accessed 21 April 2014).
- Rotzer, T., Chmielewski, F.M., 2001. Phenological maps of Europe. *Clim. Res.* 18, 249–257.
- Roy, D.P., Ju, J., Kline, K., Scaramuzza, P.L., Kovalsky, V., Hansen, M.C., Loveland, T.R., Vermote, E., Zhang, C., 2010. Web-enabled LandsatData (WELD): Landsat ETM plus composited mosaics of the conterminous United States. *Remote Sens. Environ.* 114, 35–49.
- Sieber, A., Kuemmerle, T., Prishchepov, A.V., Wendland, K.J., Baumann, M., Radloff, V.C., Baskin, L.M., Hostert, P., 2013. Landsat-based mapping of post-Soviet land-use change to assess the effectiveness of the Oksky and Mordovsky protected areas in European Russia. *Remote Sens. Environ.* 133, 38–51.
- Slater, J.A., Garvey, G., Johnston, C., Haase, J., Heady, B., Kroenung, G., Little, J., 2006. The SRM data finishing process and products. *Photogram. Eng. Remote Sens.* 72, 237–247.
- Teillet, P.M., Guindon, B., Goodenough, D.G., 1982. On the slope-aspect correction of multispectral scanner data. *Can. J. Remote Sens.* 8, 84–106.
- UN-ECE/FAO, 2000. Contribution to the Global Forest Resources Assessment 2000. Geneva Timber and Forest Study Papers, No. 17, United Nations, New York and Geneva.
- van der Linden, S., Rabe, A., Wirth, F., Suess, S., Okujeni, A., Hostert, P., 2010. ImageSVM regression, Application Manual: imageSVM version 2.1. Humboldt-Universität zu Berlin, Germany, 26 pp.
- Van Ede, R., (Unpublished M.Sc. thesis) 2004. Despeckling and geometric correction of an ASTER Level 1A Image, Utrecht University, the Netherlands, 36 pp.
- Vanonckelen, S., Lhermitte, S., Van Rompaey, A., 2013. The effect of atmospheric and topographic correction methods on forest cover classification accuracy. *Int. J. Appl. Earth Obs. Geoinform.* 24, 9–21.
- Vanonckelen, S., Lhermitte, S., Balthazar, V., Van Rompaey, A., 2014. Performance of atmospheric and topographic correction methods on Landsat imagery in mountain areas. *Int. J. Remote Sens.* 35 (13), 4952–4972.
- Vapnik, V.N., 1999. An overview of statistical learning theory. *IEEE Trans. Neural Networks* 10, 988–999.
- Veraverbeke, S., Verstraeten, W.W., Lhermitte, S., Goossens, R., 2010. Illumination effects on the differenced Normalized Burn Ratio's optimality for assessing fire severity. *Int. J. Appl. Earth Obs. Geoinform.* 12 (1), 60–70.
- Vermote, E.F., Tanré, E., Deuzé, J.L., Herman, M., Morcrette, J.J., 1997. Second simulation of the satellite signal in the solar spectrum, 6S: an overview. *IEEE Trans. Geosci. Remote Sens.* 35, 675–686.
- Vicente-Serrano, S.M., Pérez-Cabello, F., Lasanta, T., 2008. Assessment of radiometric correction techniques in analyzing vegetation variability and change using time series of Landsat images. *Remote Sens. Environ.* 112, 3916–3934.
- Vincini, M., Frazzi, E., 2003. Multitemporal evaluation of topographic normalization methods on deciduous forest TM data. *IEEE Trans. Geosci. Remote Sens.* 41, 2586–2590.
- Webster, R., Holt, S., Avis, C., 2001. The status of the Carpathians, a report developed as a part of the Carpathian Ecoregion Initiative, WWF, pp. 67.
- Zhang, Y., Yan, G., Bai, Y., 2015. Sensitivity of topographic correction to the DEM spatial scale. *IEEE Geosci. Remote Sens. Lett.* 12 (1), 53–57.
- Zhu, Z., Woodcock, C.E., 2012. Object-based cloud and cloud shadow detection in Landsat imagery. *Remote Sens. Environ.* 118, 83–94.